Pergamon

Int. J. Heat Mass Transfer. Vol. 39, No. 7, pp. 1407–1427, 1996

0017-9310/96 $15.00 + 0.00

0017-9310(95)00219-7

Natural convection in partitioned two-dimensional enclosures at higher Rayleigh numbers

K. HANJALIĆ,† S. KENJEREŠ† and F. DURST‡

† Faculty of Applied Physics, Delft University of Technology, Lorentzweg 1, 2628 Delft, The Netherlands

‡ Lehrstuhl für Strömungsmechanik, Friedrich-Alexander Universität, Erlangen-Nuremberg, Cauerstr. 4, 91058 Erlangen, Germany

(*Received* 15 *November* 1994 *and in final form* 17 *May* 1995)

Abstract—The flow pattern and the temperature field in empty and partitioned, two-dimensional (2D) rectangular enclosures were studied numerically at Rayleigh numbers 10^{10}–10^{12}, using an algebraic model for turbulent heat transport $\overline{\theta \mathbf{u}_i}$. The geometries considered, with partial, downward-extending and full adiabatic and conductive vertical partitions, imitate neighbouring rooms in real buildings with a doorway in between. Two closure levels were applied in parallel: three- and four-equation models, k–ε–$\overline{\theta^2}$ and k–ε–$\overline{\theta^2}$–ε_θ, both incorporating the low-Re-number modifications, which allow integration up to the wall and prediction of turbulence transition. The computations confirmed earlier experimental findings that in this range of Ra numbers the flow becomes turbulent, but the turbulence remains confined to only some regions of the enclosure. Noticeable improvements in capturing details of turbulence field, particularly at transitional Rayleigh numbers, are achieved with the algebraic model for turbulent heat transport $\overline{\theta \mathbf{u}_i}$, with both the three- and four-equation models, as compared with eddy diffusivity hypotheses. The paper presents some results for the mean flow and turbulence field, as well as for Nusselt number, in several cases of undivided and partitioned enclosures at transitional and higher Ra numbers and for several combinations of boundary conditions, including heating from sides and from below.

1. INTRODUCTION

Typical values of Rayleigh numbers, encountered in building enclosures, are around 10^{10} to 10^{12}. In cases with heating and cooling from sides, these values of Rayleigh number are just sufficient to promote laminar to turbulent transition along the vertical walls, but the turbulence remains usually confined to relatively narrow zones in the downstream portions of the boundary layer along each non-isothermal wall, or trapped in the regions downstream of the partition. Transition to turbulence causes a substantial increase in the heat transfer coefficient. Because the phenomenon of transition is essentially unsteady and not reproducible, experimentally obtained heat transfer correlations available in the literature for this range of Ra numbers, differ considerably. Even if the time averaged location of the transition could be defined, it depends on the Rayleigh number, so that scaling of the heat transfer for transitional Ra numbers in terms of conventional non-dimensional similarity parameters is generally very uncertain. Conductive or adiabatic partitions between the two zones of the enclosure, simulating the wall between the neighbouring rooms, with an opening imitating a doorway or a window, bring in additional uncertainties. Partitions affect substantially the flow pattern, and, depending on their position and size, may enhance or damp the turbulence and will in any case cause a redistribution of turbulence properties.

The flow pattern and turbulence intensity have a direct effect upon the indoor air quality and human comfort. In addition, transition to turbulence in boundary layers and a consequent change in the heat transfer rate will affect the moisture transport through the walls as well as vapour condensation influencing in turn the durability of the building structure. Fire and smoke spread are directly affected by the internal air circulation and turbulence intensity. Hence, adequate design of the partitions, as well as different arrangement of heating, may bring substantial improvements in building design and safety. A major prerequisite for a successful design is the ability to predict the details of the flow pattern and turbulence field and the distribution of the heat transfer coefficient along the non-isothermal walls. Similar challenge arises also in other applications, such as nuclear engineering, or in natural cooling of electric and electronic equipment, where high temperature differences may also lead to Ra numbers sufficient to promote the turbulence in spite of relatively small dimensions.

Even an empty, undivided two-dimensional (2D) enclosure possesses a number of features pertinent to complex buoyant flows. The fluid motion, induced by the buoyancy force due to the heat transfer along the

NOMENCLATURE

C	empirical coefficients in the turbulence model
$\mathbf{g}_i$	gravitation vector
h	heat transfer coefficient
H	enclosure height
H_{ob}	length of the partition measured from the ceiling
k	$0.5\overline{\mathbf{u}_i\mathbf{u}_i}$, kinetic energy of turbulence
L	enclosure length
Nu_H	$= hH/\lambda$, Nusselt number based on the enclosure height
Nu_L	$= hL/\lambda$, Nusselt number based on the enclosure length
Pe_t	$= Re_t Pr$, turbulent Peclet number
Pr	$= \nu/\alpha$, Prandtl number
Ra	= Rayleigh number
Ra_H	$= \beta g \Delta T H^3/\nu\alpha$, Rayleigh number based on the enclosure height
Ra_L	$= \beta g \Delta T L^3/\nu\alpha$, Rayleigh number based on the enclosure length
Re_t	$= k^2/\nu\varepsilon$, turbulence Reynolds number
T	mean temperature
T_o	$= \Delta T = T_h - T_c$ reference temperature scale
$\mathbf{u}_i$	turbulent fluctuation of the velocity vector
$\mathbf{U}_i$	mean velocity vector
U_o	$= (\beta g \Delta T \nu)^{1/3}$ reference velocity scale
$\overline{\mathbf{u}_i\mathbf{u}_j}$	turbulent stress tensor
$\overline{\theta\mathbf{u}_i}$	turbulent heat flux vector
w	aperture width
W	enclosure width
x_i	space coordinates
x	$= x_1$, horizontal coordinate
y	$= x_2$, vertical coordinate.

Greek symbols

α	temperature diffusivity
β	thermal expansion factor
ε	dissipation rate of the turbulence kinetic energy
ε_θ	dissipation rate of the temperature variance
$\tilde{\varepsilon}$, $\tilde{\varepsilon}_\theta$	homogeneous parts of ε and ε_θ
ξ	empirical coefficient, equation (1)
η	empirical coefficient, equation (1)
λ	thermal conductivity
μ	dynamic viscosity
ν	kinematic viscosity
ρ	fluid density
τ	k/ε, mechanical time scale of turbulence
τ_θ	$\overline{\theta^2}/2\varepsilon_\theta$, thermal time scale of turbulence
$\overline{\theta^2}$	temperature variance.

Subscripts and superscripts

h	hot wall
c	cold wall
t	turbulent.

enclosing non-adiabatic walls, is characterized by two distinct patterns: the boundary layers along the walls and the encircled recirculating motion in the core. The two patterns interact only weakly at their interface and have essentially different turbulence structure, characterized by different turbulence scales. The rotating core can develop multicellular pattern with several rolls, depending on the wall conditions, cavity aspect ratio and Rayleigh number. If the fluid is turbulent, in addition to the mean flow recirculation in form of regular-shaped rolls, turbulent fluctuations can form well organized coherent structure, pertinent particularly to the cases with heating from below. These organized motions and a strong mutual interaction between the thermal and mechanical turbulence pose a particular challenge to the modelling of the flow and heat transfer by single-point averaging closure models, which per se do not recognize any turbulence coherence.

An additional problem is the treatment of the turbulent-molecular and viscid–inviscid interactions which are often significant in some regions of the flow, even at high bulk *Ra* numbers. In fact the transition to turbulence in natural convection in enclosures occurs at relatively high *Ra* numbers and in most cases of practical relevance (space heating, flow in building structures, cooling of nuclear reactors and of electronic and electrical equipment) turbulence is significant only in some regions of the flow domain. A reliable computation model is expected to capture and reproduce not only the transition itself, but also its location and adequate dynamics of the turbulence evolution, including the turbulence decay away from solid walls. In the case of vertical non-adiabatic walls, the largest buoyancy effects are usually encountered very close to the wall where the viscous effects are still substantial and the computation of the flow and heat transfer requires a proper account of molecular effects and integration up to the wall, even though the wall boundary layer may be fully turbulent. On the other hand, free convection over horizontal heated surfaces becomes turbulent almost instantly as soon as the *Ra* number exceeds the critical value, and the momentum and heat transfer occurs through the vertical penetration of turbulent fluid due to buoyancy, irrespective of the temperature gradient in that direction.

In spite of the fact that these and other mentioned features seem hardly tractable by the current single-point closure modelling, this approach in conjunction with numerical computations still remains the only

feasible way of predicting the turbulent flow and heat transfer distribution in natural convection in complex geometries.

Natural convection in empty and partially divided, 2D and 3D enclosures has been investigated both experimentally and numerically, though in most cases the flow regime was laminar (e.g. [1–11]). Nansteel and Greif [1] investigated the problem in a small-scale laboratory 2D model of an enclosure of aspect ratio $H:L = 1:2$ with different partial division hanging from the top wall, using water ($Pr \approx 3.5$–7). The experiments were performed for Rayleigh numbers, Ra_L, based on the enclosure width L and wall temperature difference ΔT, in the range of 10^{10}–10^{11}. In all considered cases the flow remained essentially laminar, exhibiting the same flow pattern independent of the Rayleigh number for the range considered. From a later study in a 3D geometry with opening of different breadths in the partitioning wall, Nansteel and Greif [2] concluded that three-dimensionality had a strong effect upon the flow pattern behind the partition, producing at $Ra_L \approx 10^{11}$ intensive turbulence. Contrary to the 2D enclosures, the 3D partitions were found to have a destabilizing effect on the flow. However, because the turbulence remained confined to the region adjacent to the adiabatic ceiling, with boundary layer relaminarizing as soon as it encountered the cooled wall, there was a very small effect on the cross-cavity heat transfer. In view of the Prandtl number effect on the transition, one may expect a different outcome at the same Ra number with different fluids. Experiments in a similar small scale model with water, but with the aspect ratio of 1 : 3 and partitions rising from the floor and extending above the half of the enclosure height were reported by Lin and Bejan [4], who found somewhat different flow pattern with two velocity maxima in the return flow and about 50% smaller heat transfer rates than Nansteel and Greif [1]. They attributed the difference to several factors, primarily to different aspect ratio and conductivities of the partitions, but also to the measuring techniques applied and to uncontrolled heat losses. Olson *et al.* [5] reported on parallel experiments in a full-scale room of 1 : 3 aspect ratio, with air, and in a small scale model of the same geometry, using R-114 gas ($Pr \approx 0.8$), both with partitions extending from the bottom wall, for Ra_H (based on the enclosure height H) from 1.3×10^{10} to 3.4×10^{10} ($Ra_L = 4.1 - 9.8 \times 10^{11}$). They found that the flow pattern in all cases remained very similar, but detected turbulent boundary layers along all walls, as well as some secondary backward motion of the outer fluid at the beginning of the boundary layers along the hot and cold vertical walls. Although the considered geometry was three dimensional, the opening extended over the whole enclosure breadth, so that the appearance of turbulence, as compared with the laminar regime in the case of Nansteel and Greif, was probably more a consequence of higher Ra number and lower Pr number, which enhances the transition, than of the 3D effects or possible radiation influence. Neymark *et al.* [8] reported an experimental study in a cubic enclosure with an adiabatic internal partition with centrally positioned aperture extending to the half height of the enclosure, but with different relative widths w/W ranging from 0.01 to 1. They also performed a full-scale experiment with air and a small-scale experiment with water, in both cases with a constant heat flux at the hot wall, while maintaining the cold wall at a constant temperature. The Ra_H numbers considered, 5×10^{11}–5×10^{12} for air and 4×10^{11}–1×10^{13} for water are probably the highest experimentally achieved values reported so far. Flow visualization in the water experiment at $Ra = 2 \times 10^{12}$, using dye injection, showed that the boundary layer along the hot vertical wall remained laminar, though with some waviness, for both aperture widths considered, $w/W = 0.01$ and 0.2. However, in the first case, the jet-like motion exiting the aperture at about 45° upwards was apparently turbulent, but laminarized again in the downward boundary layer along the cold wall. In the second case the fluid rose along the partition in form of a laminar plume, but the boundary layer along the cold wall developed into turbulent roughly at the midheight. In the air experiment at the same Ra number with aperture width $w/W = 0.2$ the boundary layer along the hot wall was turbulent in the lower portion before it separated. On the basis of smoke visualization and hot-wire measurements at one station closer to the floor the authors concluded that the boundary layer along the cold wall was also turbulent for the range of Ra numbers considered, though they do not give any indication of the turbulence persistence over the whole wall length.

One should also mention the direct numerical simulation of natural convection in 2D and 3D partitioned cubic enclosures by Fusegi *et al.* [9] for $Ra = 10^7$ and 5×10^9, using the numerical grid distribution comparable to our study. For higher Ra the time averaging gave a substantial level of turbulent stresses, but much lower level of the temperature variance, both spread over almost the complete domain. Due to extreme requirements for computing resources the authors cautioned that they were not able to reach a fully confident statistics within the computing time available. It is interesting that the 3D computations for a partition extending across the whole cavity widths showed a great similarity with the 2D computations in regions away from the lateral walls, confirming that the effects of three-dimensionality in the central regions can be ignored.

The present paper addresses the 2D natural convection in geometries similar to those investigated experimentally by the mentioned groups of authors. The computations were performed both for water and air, for empty and partitioned enclosures, simulating the aspect ratios and Rayleigh numbers as investigated in the mentioned experiments. The cases with air had realistic dimensions and boundary conditions cor-

responding to the situations encountered in full-scale room heating. We focused on the problem of detecting the turbulent regime and performed the computations with several models, aimed at testing their capabilities for reproducing the laminar-to-turbulent and reverse transition in buoyancy driven flows, location of turbulent zones in enclosures and turbulence effect on heat transfer along the surrounding walls. Because of the lack of detailed experimental data for more complex geometries, the applied models were first verified in empty cavities of different aspect ratios and boundary conditions. As illustrated, we present a selection of results for enclosures of aspect ratio $H:L = 1:2$ and $1:3$ with differential side heating, and an $H:L = 1:1.5$ enclosure with floor heating and cooled ceiling. The effect of inserting downward hanging partitions of different height was studied in the enclosure of $H:L = 1:2$, which corresponds to the experimental case of Nansteel and Greif. Finally, results will be presented for a two zone enclosure, with a complete conductive partition, with floor heating in one zone and side cooling in the other, illustrating a more complex case with mixed boundary conditions. The model performance was validated by comparison with available experimental data for some mean properties, as well as by qualitative comparison of flow patterns, particularly the appearance and location of turbulent regions in the flow. The computed average Nusselt numbers for different geometries were also compared with the available correlations.

2. TURBULENCE MODELS

The starting point of the considered variants of turbulence models is the algebraic expression for the turbulent heat flux derived from the parent full transport equations for the turbulent heat flux

$$\overline{\theta \mathbf{u}_i} = -C\tau\left(\overline{\overline{\mathbf{u}_i\mathbf{u}_j}}\frac{\partial T}{\partial x_j} + \xi\overline{\theta\mathbf{u}_j}\frac{\partial U_i}{\partial x_j} + \eta\beta\mathbf{g}_i\overline{\theta^2}\right) \quad (1)$$

where τ is the typical time scale of turbulence, assumed as $\tau = k/\varepsilon$. The expression is closed by solving the transport differential equations for the turbulence energy k and its dissipation rate ε, with adequate modification to account for the low-Re number effects. This enables the evaluation of τ, as well as the turbulent stresses $\overline{\overline{\mathbf{u}_i\mathbf{u}_j}}$ via the eddy viscosity formulation. In nonisothermal systems, the thermal scale $\tau_\theta = \overline{\theta^2}/2\varepsilon_\theta$ governs the dynamics of thermal turbulence ($\overline{\theta^2}$ is the fluctuating temperature variance and $\varepsilon_\theta = \alpha(\overline{\partial\theta/\partial x_j})^2$ its molecular dissipation). τ_θ can be supplied from the assumed constant scale ratio $R = \tau/\tau_\theta$, or $\overline{\theta^2}$ and ε_θ can be obtained from their transport differential equations. The model for the turbulent heat flux can take various forms depending on how many and what terms in the expression (1) are retained. The simplest level considered corresponds to the isotropic eddy diffusivity model known also as the simple gradient diffusion hypothesis, $\overline{\theta\mathbf{u}_i} = -Ck^2/\varepsilon(\partial T/\partial x_i)$. This model was found inadequate for free convective flows irrespective of boundary conditions. For example, in the case of vertical non-adiabatic walls the major heat flux responsible for the turbulence generation due to buoyancy (the component in the vertical direction), is expressed in terms of relatively small vertical component of the temperature gradient. In cases heated from below a mixed layer is formed with an almost uniform mean temperature profile not much correlated with the intensive upward turbulent heat flux. The next level is the application of the non-isotropic eddy diffusivity, known also as the generalized gradient diffusion concept [essentially the first term in the expression (1)] which improved substantially the prediction of natural convection in tall cavities, but still did not produce results in full accord with the experimental data for most cases considered. Finally, we considered the complete algebraic expression (1) which accounts not only for the contribution of the mean velocity gradients, but also for the mutual interaction between the different components of the turbulent heat flux, and for the contribution due to the temperature variance [the last term in the expression (1)]. The latter is usually expressed in terms of the mean temperature gradient $\overline{\theta^2} = -C_\theta(k\overline{\theta\mathbf{u}_j}/\varepsilon)(\partial T/\partial x_j)$. However, a more detailed testing of, e.g. tall cavities with side heating and cooling revealed that only the solution of the differential transport equation for $\overline{\theta^2}$ and for its sink, $\varepsilon_\theta = \alpha(\overline{\partial\theta/\partial x_j})^2$, reproduces accurately the temperature field in all parts of the enclosures of very high and very low aspect ratios. As will be illustrated later, satisfactory results can in most cases be obtained also by omitting the transport equation for ε_θ by assuming a constant ratio of time scales $\tau_\theta/\tau \approx 0.5$, which simplifies to a great degree the application of the model to the computation of complex flows.

In order to reproduce the laminar-to-turbulent transition along the bounding walls, the model should account for molecular effects. The low-Re-number k–ε model of Jones and Launder [12] provides a reasonable framework. Although designed to model the turbulence damping in the viscous sublayer adjacent to a solid wall, the model proved to be capable of reproducing the reverse transition (laminarization) in accelerating flow, and also some cases of by-pass transition in an isothermal boundary layer, none of which is directly related to the wall vicinity. This model is one of few among many of a kind, in which the damping functions are expressed in terms of an invariant property, the turbulence Reynolds number $Re = k^2/\nu\varepsilon$, not dependent directly on the distance from the wall, nor on wall topography. This feature is important for modelling natural convection at transitional Rayleigh numbers, with weak turbulence field appearing only in some regions of the flow domain. Accurate prediction of the turbulence interaction with non-turbulent fluid away from the wall may require additional modification of the model and its verification in the prediction of homogeneous buoyant turbulence.

However, any model deficiency in this respect may only influence the results in the outer edge of the turbulence zone where the turbulent fluctuations of velocity and temperature decay freely, without affecting much the mean velocity and temperature field, nor wall heat transfer. Following these arguments we have adopted Jones–Launder–Sharma low-*Re*-modifications for the k and ε equation and analogous modifications for molecular effect in the $\overline{\theta^2}$ and ε_θ equations. These modifications are expected to provide for the molecular and wall effects on turbulent heat flux $\overline{\theta \mathbf{u}_i}$ through the adjustment of the time scale τ and other variables in equation (1). This approach may not satisfy the exact conditions at the wall. To meet these constraints, the equation (1) should include the term $\varepsilon_{\theta i}$ which has been neglected here and the coefficient C replaced by a function in terms of turbulent Peclet number. However, the expression (1) in conjunction with the three- and four-equation models here considered, showed to reproduce well the natural convection in a boundary layer along the heated vertical plate and in rectangular cavities (Hanjalić and Vasić, [13]) and was adopted in the present work.

The following set of equations in conjunction with expression (1) constitute the adopted model:

$$\frac{\mathrm{D}(\rho\overline{\theta^2})}{\mathrm{D}t} = D_\theta + 2\rho P_\theta - 2\rho\varepsilon_\theta \tag{2}$$

$$\frac{\mathrm{D}(\rho k)}{\mathrm{D}t} = D_k + \rho P + \rho G - \rho\varepsilon \tag{3}$$

$$\frac{\mathrm{D}(\rho\tilde{\varepsilon})}{\mathrm{D}t} = D_\varepsilon + C_{\varepsilon 1}\rho(P+G)\frac{\tilde{\varepsilon}}{k} - C_{\varepsilon 2} f_\varepsilon \rho \frac{\tilde{\varepsilon}^2}{k} + E + S_l \tag{4}$$

$$\frac{\mathrm{D}(\rho\tilde{\varepsilon}_\theta)}{\mathrm{D}t} = D_{\varepsilon\theta} + C^\theta_{\varepsilon 1}\rho P\frac{\tilde{\varepsilon}_\theta}{k} + C^\theta_{\varepsilon 3}\rho P_\theta \frac{\tilde{\varepsilon}_\theta}{\theta^2} - C^\theta_{\varepsilon 2}\rho\frac{\tilde{\varepsilon}_\theta^2}{\overline{\theta^2}} - C^\theta_{\varepsilon 4} f_{\varepsilon\theta}\rho\frac{\tilde{\varepsilon}_\theta\tilde{\varepsilon}}{k} + E_\theta \tag{5}$$

where

$$P = -\overline{\mathbf{u}_i\mathbf{u}_j}\frac{\partial \mathbf{U}_i}{\partial x_j}, \quad G = -\beta \mathbf{g}_i \overline{\theta \mathbf{u}_i}; \quad P_\theta = -\overline{\theta \mathbf{u}_j}\frac{\partial T}{\partial x_j}; \tag{6}$$

$$E = 2\mu\frac{\mu_t}{\rho}\left(\frac{\partial^2 \mathbf{U}_i}{\partial x_j \partial x_k}\right)^2 \quad E_\theta = 2\rho\alpha\alpha_t\left(\frac{\partial^2 T}{\partial x_j \partial x_k}\right)^2 \tag{7}$$

$$\tilde{\varepsilon} = \varepsilon - 2\nu\left(\frac{\partial (k)^{1/2}}{\partial x_n}\right)^2 \quad \tilde{\varepsilon}_\theta = \varepsilon_\theta - \alpha\left(\frac{\partial(\overline{\theta^2})^{1/2}}{\partial x_n}\right)^2 \tag{8}$$

$$D_\phi = \frac{\partial}{\partial x_j}\left(C_\phi f_\mu \rho \frac{k^2}{\tilde{\varepsilon}}\frac{\partial \phi}{\partial x_j} + \mu\frac{\partial \phi}{\partial x_j}\right) \tag{9}$$

$$S_l = 0.85\left(\frac{l_e}{l} - 1\right)\left(\frac{l_e}{l}\right)^2 \frac{\tilde{\varepsilon}^2}{k} \tag{10}$$

where $L_l = k^{3/2}/\varepsilon$ and $l = 2.5x_n$. The model contains the two damping functions:

$$f_\mu = \exp\left[\frac{-3.4}{\left(1+\frac{Re_t}{50}\right)^2}\right] \quad f_\varepsilon = 1 - 0.3\exp(-Re_t^2). \tag{11}$$

Here P and G stand for the turbulence energy production by strain and buoyancy respectively, P_θ is the production of temperature variance, while E and E_θ account for molecular effects. D denotes the total diffusion term in which the turbulent part was modelled by the simple gradient hypothesis. The last term, S_l in the $\tilde{\varepsilon}$ equation is the correction attributed to Yap, (Ince and Launder, [14]), which damps the excessive growth of the length scale close to the wall and was found to improve the reproduction of the dissipation in the wall vicinity as well as numerical stability. It should be mentioned that the model can give similar results by omitting S_l term, but the coefficient C has to be slightly adjusted. Turbulent stresses were computed from the eddy viscosity expression

$$\overline{\mathbf{u}_i\mathbf{u}_j} = \tfrac{2}{3}k\delta_{ij} - \nu_t\left(\frac{\partial \mathbf{U}_i}{\partial x_j} + \frac{\partial \mathbf{U}_j}{\partial x_i}\right),$$

where $\nu_t = 0.09\, f_\mu k^2/\tilde{\varepsilon}$. The function $f_{\varepsilon\theta}(Pe_t)$ should ensure a transition from the initial to the final stage of decay of the temperature variance when Pe_t falls bellow the critical value in the same manner as the function f_ε does for the velocity fluctuations. In absence of reliable data for model validation, this function was assumed 1, in anticipation that for fluids with Pr numbers close to unity, the thermal turbulence will follow closely the dynamics of the mechanical turbulence. Any inadequacy in this assumption may only marginally influence the predictions of the turbulence field at the very edge of a turbulence region. The following coefficients were adopted.

C	ξ	η	C_ε	$C_{\varepsilon 1}$	$C_{\varepsilon 2}$	C^θ_ε	$C^\theta_{\varepsilon 1}$	$C^\theta_{\varepsilon 2}$	$C^\theta_{\varepsilon 3}$	$C^\theta_{\varepsilon 4}$
0.2	0.6	0.6	0.07	1.44	1.92	0.07	0.72	2.2	1.3	0.8

3. NUMERICAL METHOD

Numerical computations were performed by a version of finite volume Navier–Stokes solver for 2D flows in orthogonal coordinate system, adopted from Demirdžić and Perić (e.g. [15]). Staggered grid, clustered toward the walls was employed with typically 80–120 grid points in both coordinate direction for each zone on both sides of the partition. SIMPLE algorithm was used for the treatment of the pressure field. The solutions were obtained by false time marching, employing the Stone's strongly implicit iterative lower/upper (ILU) method. More details about the testing of the applied numerical method for natural convection were reported in ref. [16].

4. SOME RESULTS

In order to illustrate the performances of the model, we present first some results for empty enclosures with moderate aspect ratios between 1 : 1 and 1 : 3, which correspond more closely to situations encountered in room heating. Two types of typical boundary conditions have been considered: differential heating of the vertical side walls and differential heating of horizontal walls from below. In both cases the remaining two walls were kept adiabatic.

4.1. *Undivided short enclosures with bottom heating*

The first example is an enclosure with aspect ratio $H:L = 1:1.5$ with heated floor and cooled ceiling. Unlike in side-heated enclosures, where the turbulence may occupy only a portion of the flow domain, in the case with heating from below the fluid in the enclosure becomes turbulent in the whole flow domain as soon as the Ra number reaches the critical value of $\approx 5 \times 10^4$ (here the Ra number is defined with the enclosure height H which is the natural characteristic dimension of the flow). In slender horizontal enclosures of small aspect ratio, $H:L \ll 1$, the regular laminar roll-cells break, to be replaced by thermals rising vertically. It is generally believed that in a fully turbulent regime in slender domains, like in the case of parallel infinite plates, no cellular patter exists and the statistical averages of the properties vary only in the vertical direction. However, it has been noticed, e.g. by Chu and Goldstein [17], that a further increase in the Ra number above the critical value will induce a horizontal fluid motion along the horizontal boundaries from which thermals break periodically, upwards from the bottom wall and downwards from the top one, *at relatively fixed sites*. This suggests that a pair of thermals may create a rotating roll so that in the turbulent regime also the flow pattern takes the form of a series of roll-cells, though not so orderly as in the laminar regime, and not so easily detectable by visualization technique due to strong fluctuation of the velocity and temperature field. The formation of roll-cells will be enhanced by the side walls in enclosures and the effect will be stronger if the side walls are closer, i.e. at moderate aspect ratios. In enclosures with aspect ratio close to unity, at lower Ra numbers the flow pattern may develop more than one cell due to shorter periods of instability at which thermals part from the boundary layers, but at higher Ra numbers the momentum of the horizontal motion increases and the enclosure is filled basically with a single roll occupying almost the whole flow domain, with possibly some small secondary rolls in the corners. The dominant rotating motion can take any direction of rotation. In nature the direction will depend on the initial disturbances, whereas in numerical computations starting with a uniform field and boundary conditions, it will take the direction in which the solution sweeps are performed.

Of course, none of the sort of organized unsteady patterns can be reproduced by single-point model based on Reynolds averaging. Higher order turbulence models have shown to reproduce the statistically averaged mean temperature and turbulence field in 1D steady and unsteady buoyant convection over a heated horizontal plate or between the two infinite plates featuring strong temperature gradients in the vicinity of both horizontal walls and a well mixed core with almost uniform distribution of the mean temperature and linear vertical turbulent heat flux, in good agreement with experiments (Hanjalić and Vasić, [13]). In the case of short enclosures, the 2D numerical computations yield invariably a circular motion of the bulk flow and this pattern persists at much higher Ra numbers, than reported in experiments. Indeed, at high Ra numbers the flow visualization becomes difficult and not much information can be found in literature for higher Ra numbers. Besides, in most experimental works the measurements are taken only at one cross-section, usually in the middle of the enclosure and no exploration of the horizontal variation of flow properties, nor are details in the enclosure corners are known to us. We believe, therefore, that the computed rotating pattern in short enclosures, even at relatively high Ra numbers with strong turbulence, may correspond to reality. As an illustration, Fig. 1 shows the results of computations of some of the properties for $Ra = 10^8$, obtained by the four-equation model.

As seen, in spite of a relatively short width, in the bulk portion of the flow, excluding the corners, the variation of flow properties in horizontal direction is almost negligible. All thermal properties show high gradients in the wall boundary layers, with almost uniform distribution in the enclosure core. Figure 2 shows the computed temperature profiles for a range of Ra numbers, from 10^6 to 10^{10}. The measurements by Chu and Goldstein [17], for $Ra = 4 \times 10^5$ are also shown for comparison. It is interesting to note that the mean temperature exhibits an inversion, as found experimentally by Chu and Goldstein, which is in fact a consequence of the rotating motion.

Another interesting feature is the diagonal symmetry of the flow pattern, in spite of the vertical symmetry of the enclosure geometry and boundary conditions. The flow pattern tends to develop small secondary rolls in the downstream corners of each adiabatic vertical wall, as shown in Fig. 1 for $Ra = 10^8$. These secondary rolls and the adjacent portions of the boundary layers on the horizontal non-adiabatic walls are characterized by a high concentration of both the mechanical and thermal turbulence, particularly of $\overline{\theta^2}$ and $\overline{\boldsymbol{\theta}\mathbf{u}_2}$, enhancing the heat transfer on non-adiabatic walls, as illustrated by conspicuous peaks of the Nusselt number, Fig. 3. Less pronounced peaks of the Nusselt number appear also in the downstream ends of the boundary layers. It is interesting to note that at higher Ra numbers, like in the case for $Ra = 10^9$, the distribution of the Nusselt number is more uniform over the large portion of the wall with peaks in the upstream regions of the wall

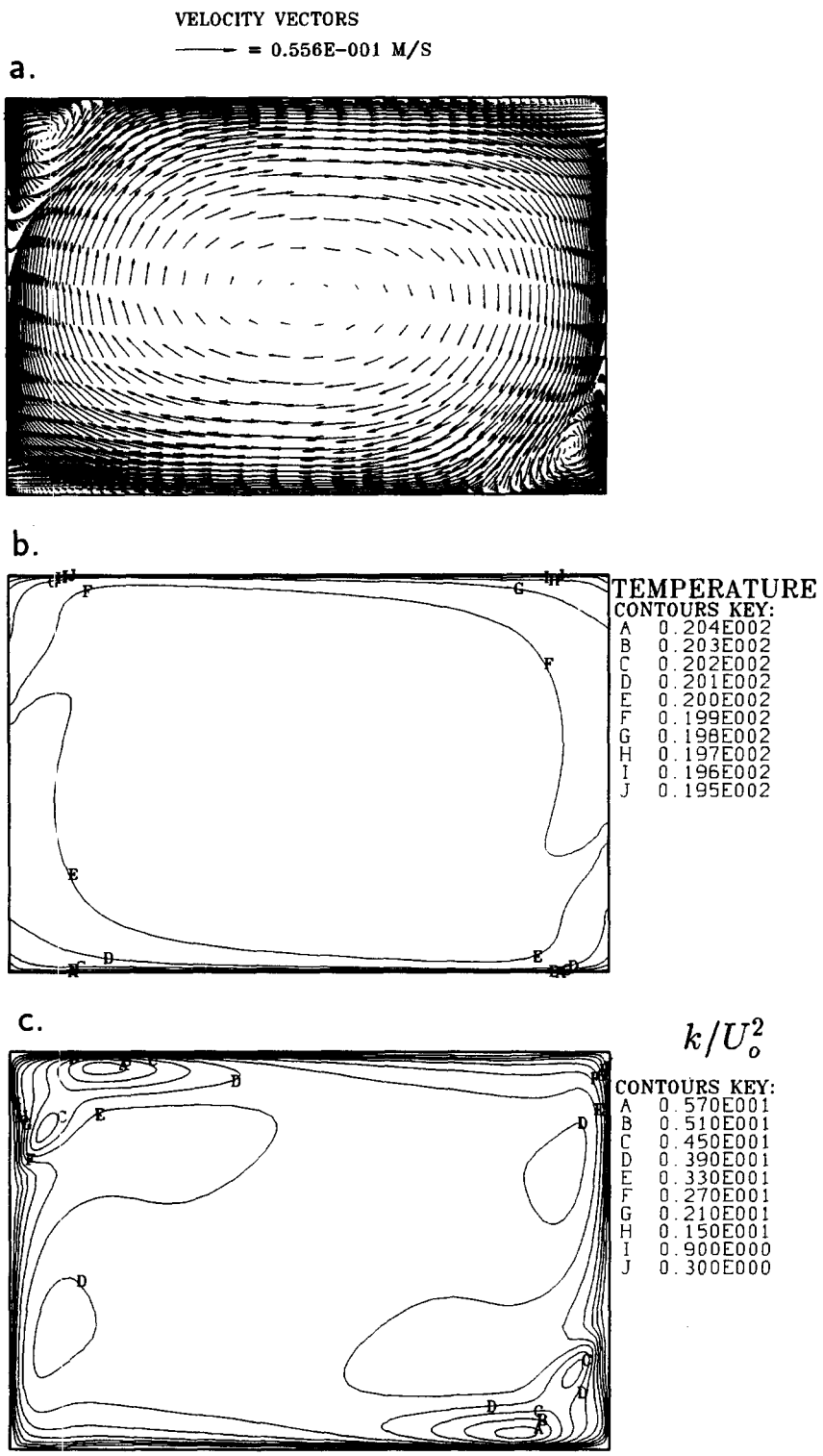

Fig. 1. Computed mean and turbulence properties in a rectangular enclosure heated from below, $H:L = 1:1.5$, $Ra = 10^8$.

boundary layer just after the fluid encounters the non-adiabatic wall, whereas the secondary peaks at the end of the boundary layers disappear completely. Like in other examples with different aspect ratio (e.g. Hanjalić [18]), especially in cases with heating from below, these findings substantiate the importance of field computations for each particular case and *Ra* number, if the application requires a more accurate knowledge

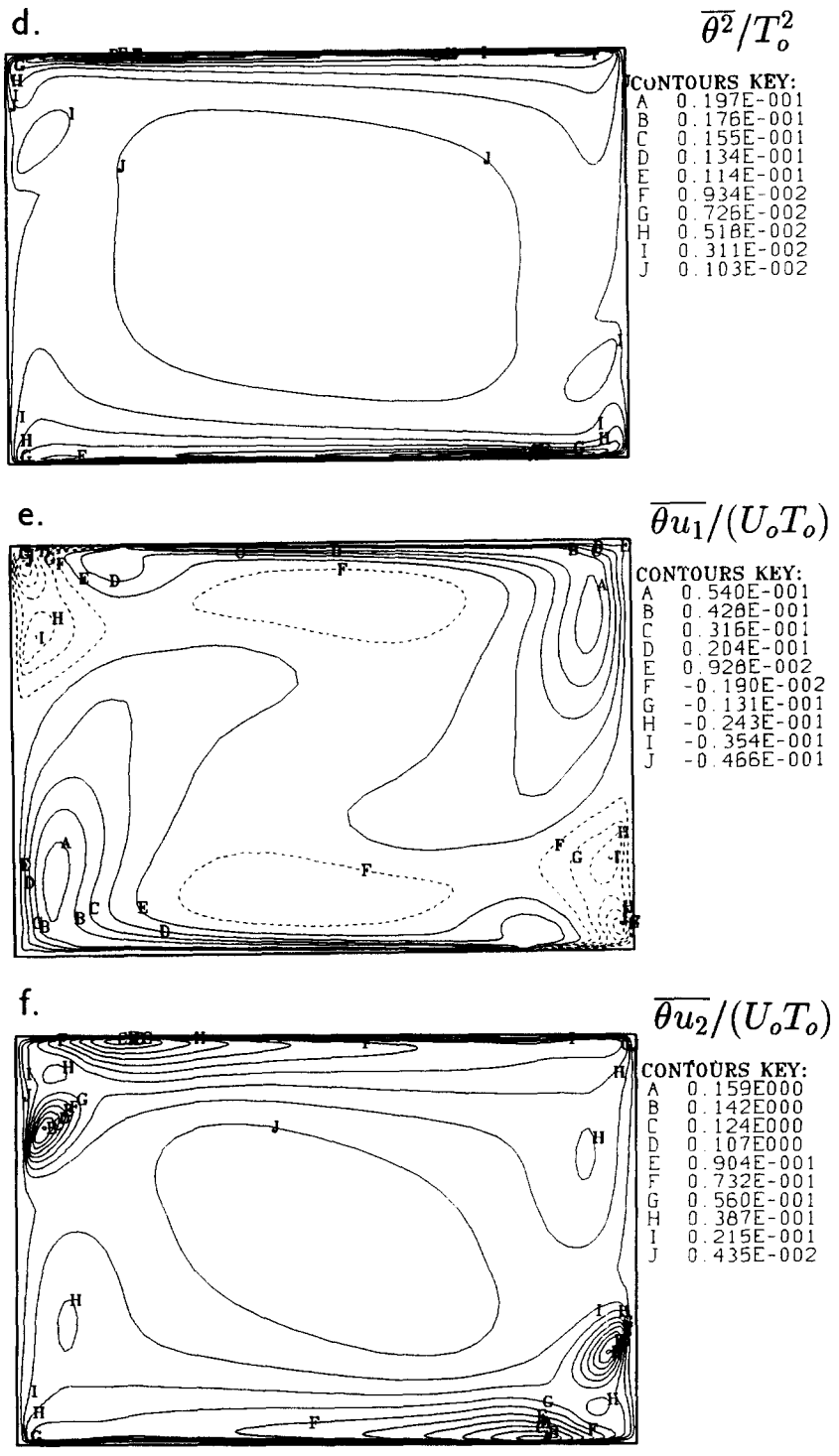

Fig. 1—*continued.*

of the heat transfer distribution along the non-adiabatic walls.

The lack of experimental or other data for field properties does not leave much opportunity for verifying the computed field results, except to compare the computed average Nusselt numbers with several correlations, available in literature. Two correlations proposed by Chu and Goldstein, $Nu = 0.123Ra^{0.294}$ for air [19], and $Nu = 0.183Ra^{0.278}$ for water [17], both obtained for a range of aspect ratios, including the 1 : 1.5, here considered, and claimed to be valid for $Ra \leqslant 10^8$, agree well with our results for lower

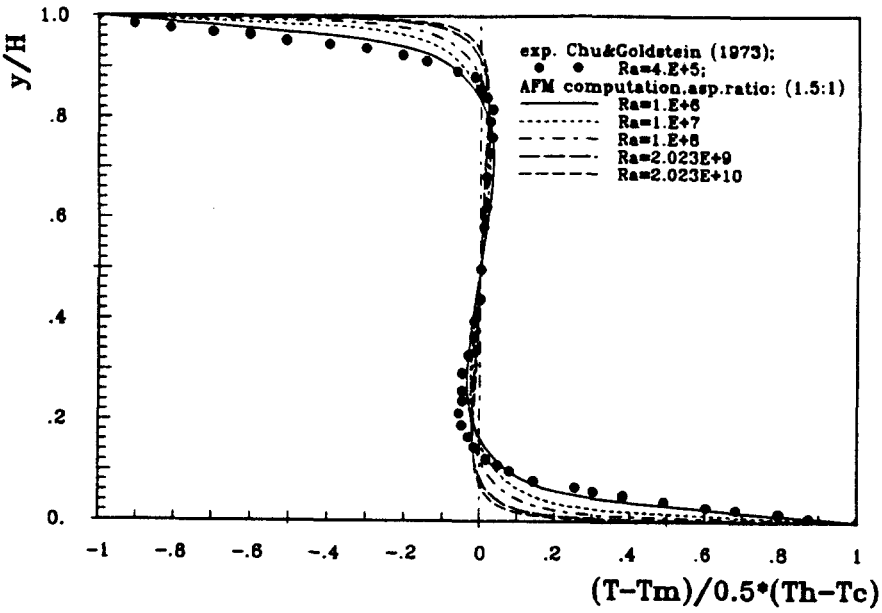

Fig. 2. Computed temperature profiles in the vertical cross-section at the middle of the enclosure heated from below, $H:L = 1:1.5$, $Ra = 10^6$–10^{10}.

Ra numbers. For example, for $Ra = 10^6$ and 10^7 the computations yielded the averaged Nusselt numbers 7.7 and 16.2, respectively, as compared to 7.14 and 14.1, obtained from the correlation for air, or to 8.52 and 16.16, obtained by the correlation for water. However, for higher *Ra* numbers the discrepancy increases. Other expressions available in literature (see e.g. Gebhart *et al.* [20]) give similar, though somewhat lower values, but still within the 15% at these two *Ra* numbers. At higher *Ra* numbers our results agree better with correlations which use higher exponent of the *Ra* number (closer to 1/3), as implied, e.g. by the correlation of Dropkin and Somercales (1965) (in [20]), Fig. 4.

The overall agreement can be regarded as satisfactory, qualifying the model for use in more complex geometries. Very similar results, particularly for the Nusselt number distribution, were obtained by the three-equation model, with a constant time scale ratio $R = 0.5$, Fig. 3(b), though the distribution of R, obtained from the four-equation model varies considerably in the enclosure domain. This illustrates a relative insensitivity of the model, at least in these simple geometries, to the choice of R, which is rather fortunate, since the three-equation model is much simpler to use and involves less number of empirical coefficients and associated uncertainty. In view of the need to arrive at a model which can be applied to 3D domains of complex geometry, this finding is regarded as very useful and further presentation of the results will be confined mostly to those obtained with the three-equation algebraic flux model. It should be pointed out, however, that the use of the isotropic eddy diffusivity (denoted as SGDH) model resulted also in reasonably good agreement at lower *Ra* numbers, but always yielded smaller Nusselt numbers, with the difference progressively increasing as the *Ra* number increases, as shown in Fig. 4.

4.2. *Undivided enclosures with side heating*

We move now to consider the side heated empty and partitioned cavities. The first in this series of examples is a 2D side heated 1 : 3 rectangular enclosure, representing a typical empty building space with realistic dimensions, $H = 2.5$ m, $L = 7.9$ m and side wall temperatures of ≈ 30 and 10°C, yielding the Ra_H of 3×10^{10} ($Ra_l \approx 9.5 \times 10^{11}$).† This case was selected to match the experimentally investigated full-scale room of Olson *et al.* [5]. Although Oslon *et al.* detected some sort of turbulence, our computations using various models yielded laminar solutions irrespective of the initially imposed turbulence field. By increasing the Ra_H to $\approx 1.5 \times 10^{11}$ the algebraic model with both, the three and four scalar transport equations, yielded solution with a weak turbulence field concentrated in the downstream portions of the boundary layers along the vertical non-adiabatic walls, but the flow pattern remained generally the same as for the laminar solution. The case appeared to be numerically very challenging because of a weak communication between the hot and cold wall over the span of three heights. Figure 5 illustrates some interesting features of the velocity and temperature field which agree qualitatively with those observed by Olson *et al.* [5]. Strong wall-jet like motion develops along all walls, with an

† Unlike in the case with heating from below, for side heated enclosures both the height H and the length (width) L of the enclosures are employed in literature for defining the Rayleigh number. For comparison with experimental data, both definitions are used in the text that follows.

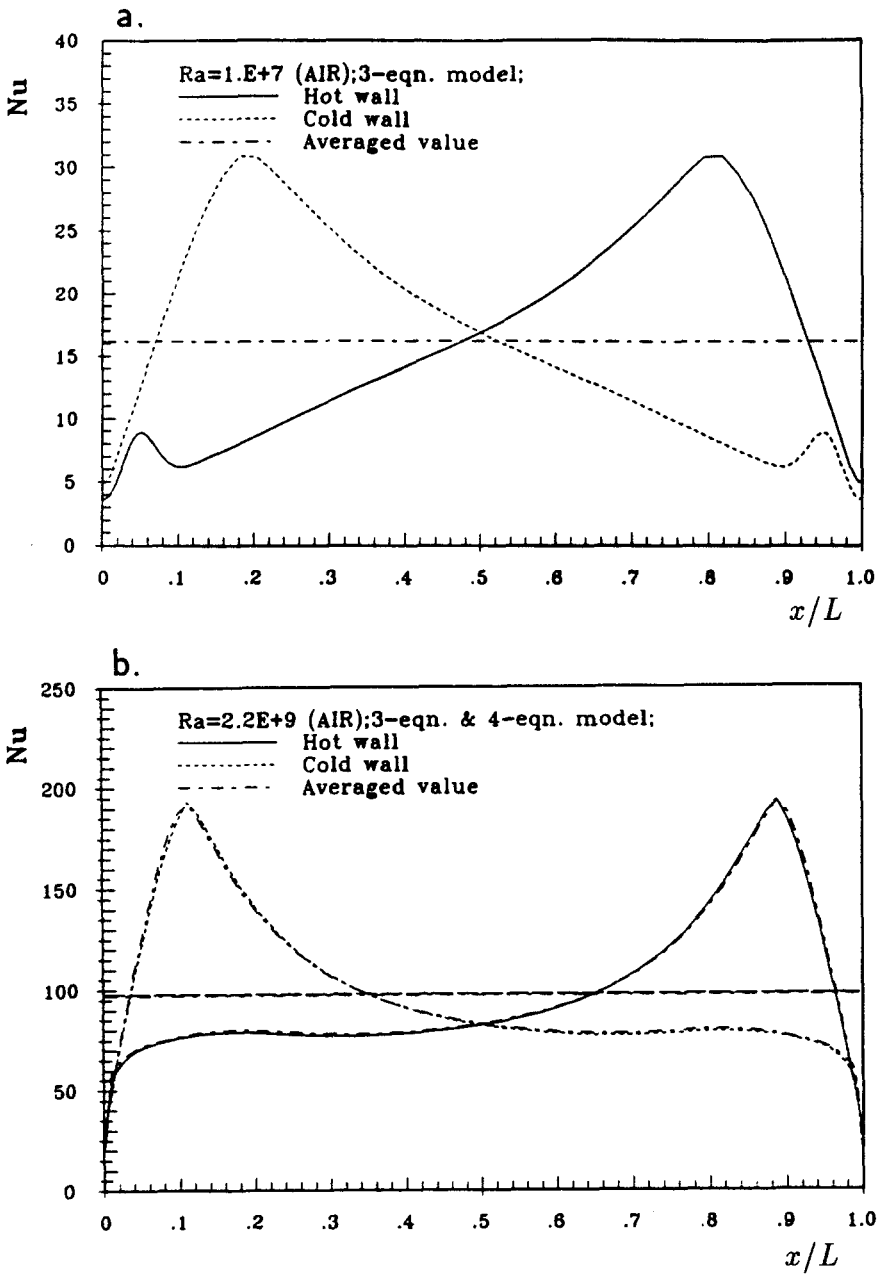

Fig. 3. Nusselt number distribution along the bottom and top non-adiabatic walls in an enclosure with $H:L = 1.5$. (a) $Ra_H = 10^7$ and (b) $Ra_H = 2.2 \times 10^9$.

almost stagnant core region. The boundary layers along the horizontal walls are visibly thicker than those along the vertical walls. However, contrary to the common perception of unidirectional flow along all walls, the computations produced two loops with backflows in the downstream regions of boundary layers along the vertical walls, and thin recirculating regions adjacent to the horizontal walls in the upper left corner (near the hot wall) and lower right corner (near the cold wall), Fig. 5(b). Due to intensive heating, the fluid adjacent to the hot vertical wall accelerates continuously, reaching the maximum velocity in the corner just before hitting the upper horizontal adiabatic wall. Strong momentum drives the fluid within the boundary layer too fast to be fully heated, so that its outer mass remains cooler and heavier than the inner layer, but also cooler than the outer core fluid, causing its downward motion. The same antisymmetric flow pattern occurs along the cold wall. This backflow is more pronounced at higher *Ra* numbers and in the turbulent regime.

A similar flow pattern was observed experimentally by Olson *et al.* [5], except that the turning of the fluid backwards occurred earlier along the wall.

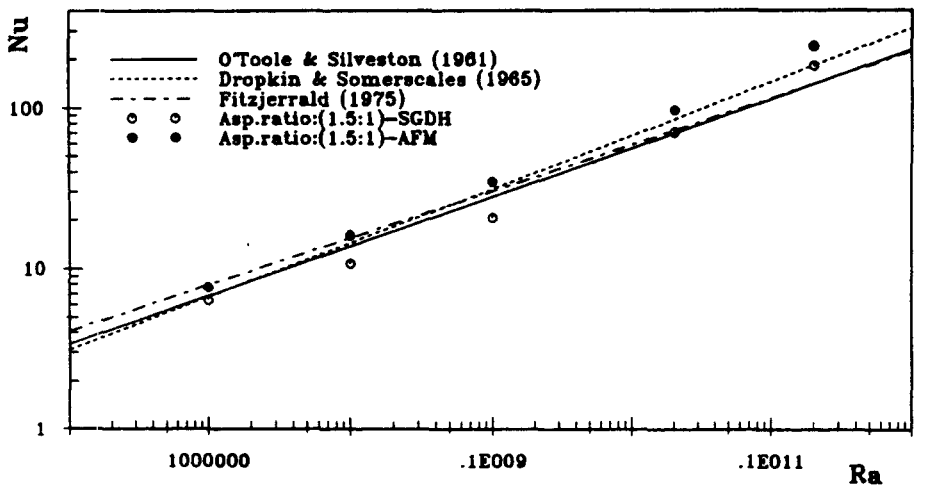

Fig. 4. Comparison of the computed Nu (Ra) results with several correlations for a 2D enclosure, heated from below, $H:L = 1.5$.

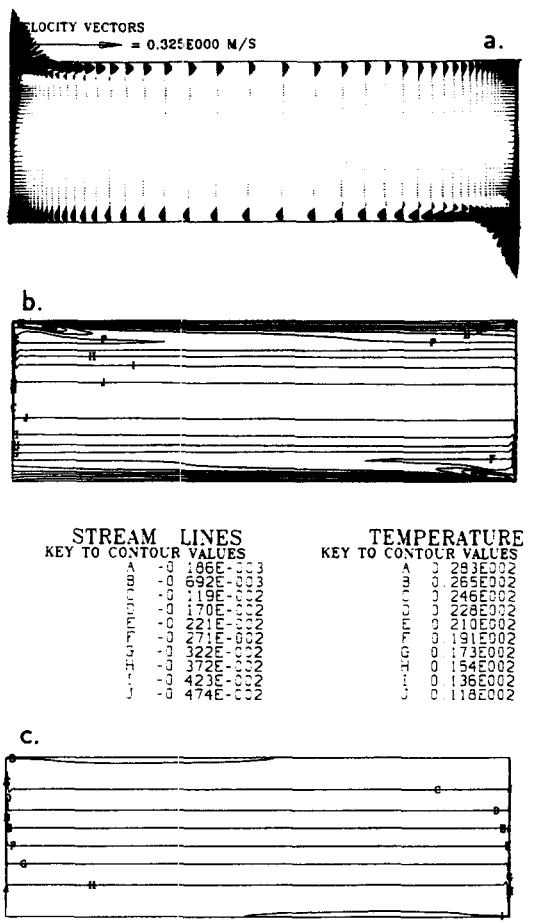

Fig. 5. Computed velocity vectors (a), streamlines (b) and isotherms (c) in a side heated 1 : 3 cavity at $Ra_H = 3 \times 10^{10}$.

The computed Nusselt numbers at several Ra numbers, including both the laminar and turbulent regimes, agree well with the available correlations, particularly for lower Ra numbers. For $Ra_H = 3 \times 10^{10}$ (laminar regime) the computed Nusselt number of $Nu_H = 131$ agrees within 1% with the correlation $Nu_H = 0.31 Ra_H^{0.25}$ of Bohn *et al.* (1984) and within 6% with the correlation $Nu_H = 0.60 Ra_H^{0.226}$ of Nansteel and Greif [1] for 2D enclosures. For $Ra_H = 1.5 \times 10^{11}$ the computed Nu_H was about 14% higher than the value from the above mentioned laminar flow correlation of Nansteel and Greif, which is expected in view of the fact that our computations produced turbulence at this Ra number.

We consider next the enclosures of a more moderate aspect ratio, $H:L = 1:2$, which served as a basic configuration for the investigation of partitioned side-heated enclosures by Nansteel and Greif [1, 2], Fig. 6. The dimensions $H = 3.65$ and $L = 7.30$ m and the wall temperatures $T_h = 35$ and $T_c = 5°C$, yield the Rayleigh number based on the cavity length $Ra_L = 1.2 \times 10^{12}$ ($Ra_H = 1.5 \times 10^{11}$). These parameters have been selected to simulate a higher Ra number situation encountered in space heating. This Ra number is almost one order of magnitude higher than in the small-scale water experiment of Nansteel and Greif [1, 2], but close to the full scale experiment of Olson *et al.* It should be recalled that Nansteel and Greif [1] invariably found laminar flow in 2D enclosures with or without partition in the range of Ra numbers considered. Our computations for the same Ra numbers also yielded laminar solutions irrespective of the initial turbulence field, which agreed very well with the measurements and observed pattern of Nansteel and Greif (Hanjalić and Vasić [10]). However, when using air and enclosure dimensions and temperatures corresponding to a full scale application, the computations showed a persistent turbulence, though confined to very narrow regions adjacent to the walls, as illustrated by the contours of turbulence Reynolds number $Re_t = k^2/v\varepsilon$, Fig. 6(d) (similar patterns follow other turbulence parameters, not shown here: turbulent kinetic energy k, temperature variance $\overline{\theta^2}$ and

component of the turbulent heat flux $\overline{\theta u_1}$ and $\overline{\theta u_2}$). Significant turbulence is concentrated in the upper region of the hot wall and in the lower region next to the cold wall. Note that the contour values have been selected with constant increment to avoid any arbitrariness in representing the extent of significant values of considered properties. With respect to this, it is interesting to note that the turbulent *Re* number extends considerably further into the 'nonturbulent' fluid than the kinetic energy itself (or the temperature variance), due to a large increase of the length scale at the edge of turbulent zones.

Unlike a simple recirculation along the walls with almost stagnant core, as usually assumed in empty enclosures, the computed flow pattern displays two loops with reverse motions in the outer parts of the wall layers, adjacent to the downstream parts of both vertical walls, Fig. 6(a) and (b). This flow reversal generates a shearing transverse motion at the mid-height plane of the enclosure, which was not detected in the previous case with 1 : 3 aspect ratio. Along the horizontal adiabatic walls the flow develops in a wall-jet type of boundary layer. After encountering the hot wall, the boundary layer at the floor turns upward. Transition to turbulence is detected around the mid-height. Although the heat transfer is enhanced by turbulence, as in the previous case with $H:L = 1:3$ it does not seem to be sufficient to heat the complete mass of fluid within the boundary layer so that the low-momentum outer fluid, cooler then the fluid in the inner wall layer, but also than the fluid in the enclosure core, turns downwards in the form of an accelerating jet. This downward motion encounters the cooler fluid from below and close to the enclosure midheight turns into the horizontal direction toward the cold wall across the central portion of the enclosure. An antisymmetric pattern develops in the cold wall region. It is interesting that the computations produced the largest velocities in the backflow just before the fluid turns toward the opposite wall. Another peculiarity is the shear layer in the central zone of the enclosure. This backflow of the outer fluid along the vertical walls resembles closely that found by Olson *et al.* [5] in their 1 : 3 cavity, but their backflow was weaker, extending at a shorter distance before turning toward the opposite wall, so that in their case two loops, separated by a stagnant core, were detected. In the experiments the counter motion of the fluid occurs in a layer adjacent to the wall boundary layer along the horizontal walls, whereas our computation for 1 : 2 aspect ratio yielded a recirculating motion with two stagnant cores separated by a shear interface at the enclosure midheight. It is difficult to say how realistic are these predictions, but this pattern was obtained with all models tested.

The computations yielded the Nusselt number of 470, which is about 14% larger from the value obtained from the correlation of Nansteel and Greif [1] for 2D laminar convection at the same *Ra* number. Because our computations produced some turbulence

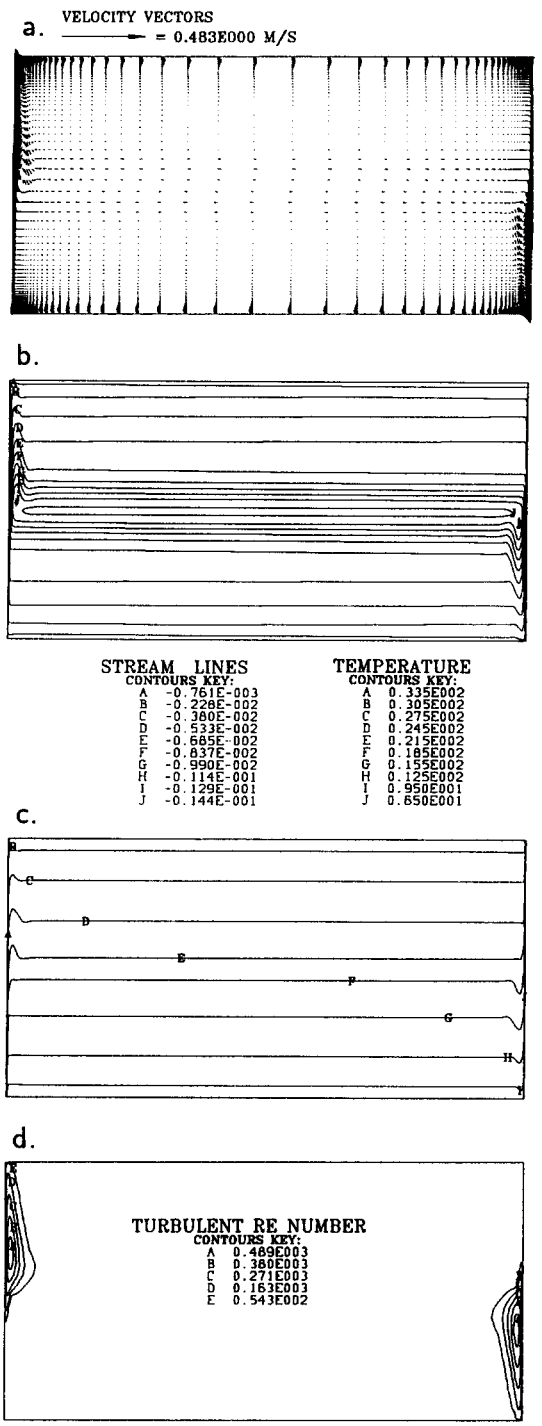

Fig. 6. Computed mean and turbulence properties in a rectangular enclosure heated differentially from sides, $H:L = 1:2$, $Ra_L = 1.2 \times 10^{12}$; (a) velocity vectors; (b) streamlines; (c) isotherms and (d) turbulence Reynolds number, Re_t.

along the non-adiabatic walls, the larger Nusselt number is expected. A similar increase in the Nusselt number was reported by Olson *et al.* who detected turbulent regime in their experiments. It should be noted that our computations of Olson *et al.* empty enclosure

for somewhat smaller Ra number ($Ra_L = 9.8 \times 10^{11}$) gave a laminar solution with small recirculations in the initial portion of flow along the horizontal walls, resembling, at least in this region (but without a vertical backflow), the pattern depicted by Olson *et al.* The computed $Nu_L = 414$ agrees within 1% with the correlation $Nu_H = 0.31 Ra_H^{0.25}$ of Bohn *et al.* [21] and within 6% with correlations for 2D and 3D enclosures of Nansteel and Greif [1, 2], $Nu_H = 0.60 Ra_H^{0.226}$ and $Nu_L = 0.762 Ra_L^{0.226}$, respectively.

4.3. *Partially divided enclosures with side heating*

Inserting an incomplete partition, suspended from the ceiling, or protruding upwards from the floor, causes substantial changes in flow patterns. At $Ra = O(10^{10})$ Nansteel and Greif detected laminar flow both in the 2D and 3D enclosures. In the first case the flow remained almost fully attached to the wall, bending sharply upwards after the partition, whereas in 3D cases with small opening breadth, the flow displayed a separation at the partition tip, as well as from the ceiling in the upper corner adjacent to the cold wall, before turning downwards. At $Ra_L = O(10^{11})$ their experiments showed no turbulence in the 2D geometry, whereas in the 3D flow transition occurred behind the partition at its intersection with the ceiling, producing an intensive turbulence in the complete upper zone of the right part of the enclosure. Similar effects of the aperture in a 3D enclosure was detected by Neumark *et al.* [8], except that in their experiments at $Ra = 2 \times 10^{12}$ with air they detected turbulence in the ascending boundary layer on the hot wall.

Our computations for $Ra_L = 1.2 \times 10^{12}$ and with adiabatic partitions of different lengths, $H_{ob}/H = 0$–0.75, with H_{ob}/H increments of 0.125 (where H_{ob} is the length of the partition measured from the ceiling), showed the presence of turbulent zones for all cases for $H_{ob}/H < 0.5$, in accord with the findings of Neumark *et al.* [8], though the location of turbulent zones was different, as shown in Figs. 7 and 8 for $H_{ob}/H = 0.25$ and 0.5, whereas for higher H_{ob}/H the turbulence disappeared completely, as shown in Fig. 9 for $H_{ob}/H = 0.75$.

The streamline patterns look, however, similar. Along the hot wall the flow resembles that in an empty cavity with a loop-form downward backflow of the outer fluid which turns into a horizontal jet-like motion at the height just below the partition tip. Only a small portion of the fluid continues to flow along the hot wall, generating a very weak laminar circulation in the upper zone of the enclosure next to the hot wall. In the case of $H_{ob}/H = 0.25$ a portion of fluid continues to move downwards and then turns horizontally toward the cold wall, forming a weak shear layer roughly in the midzone of the lower unobstructed part of the enclosure. In this case the turbulence is confined to the regions adjacent to vertical walls. In the case of $H_{ob}/H = 0.5$ the jet-like horizontal motion at the cavity midplane entrains almost all fluid

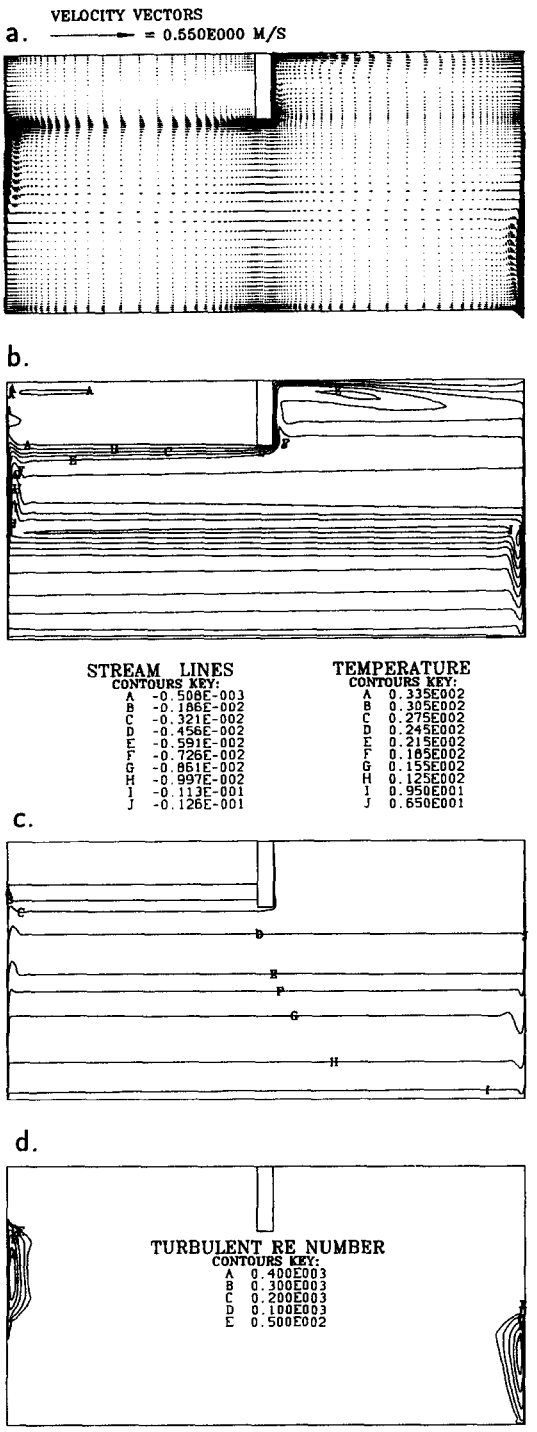

Fig. 7. Computed mean and turbulence properties in a partially divided side heated rectangular enclosure, $H:L = 1:2$, $H_{ob}/H = 0.25$, $Ra_L = 1.2 \times 10^{12}$; (a) velocity vectors; (b) streamlines; (c) isotherms and (d) turbulence Reynolds number, Re_t.

from the boundary layer, so that the upper left region of the enclosure is almost stagnant. There is also very little air movement in the core of the lower unobstructed portion of the enclosure, so that the whole hot-wall zone of the cavity is practically non-turbu-

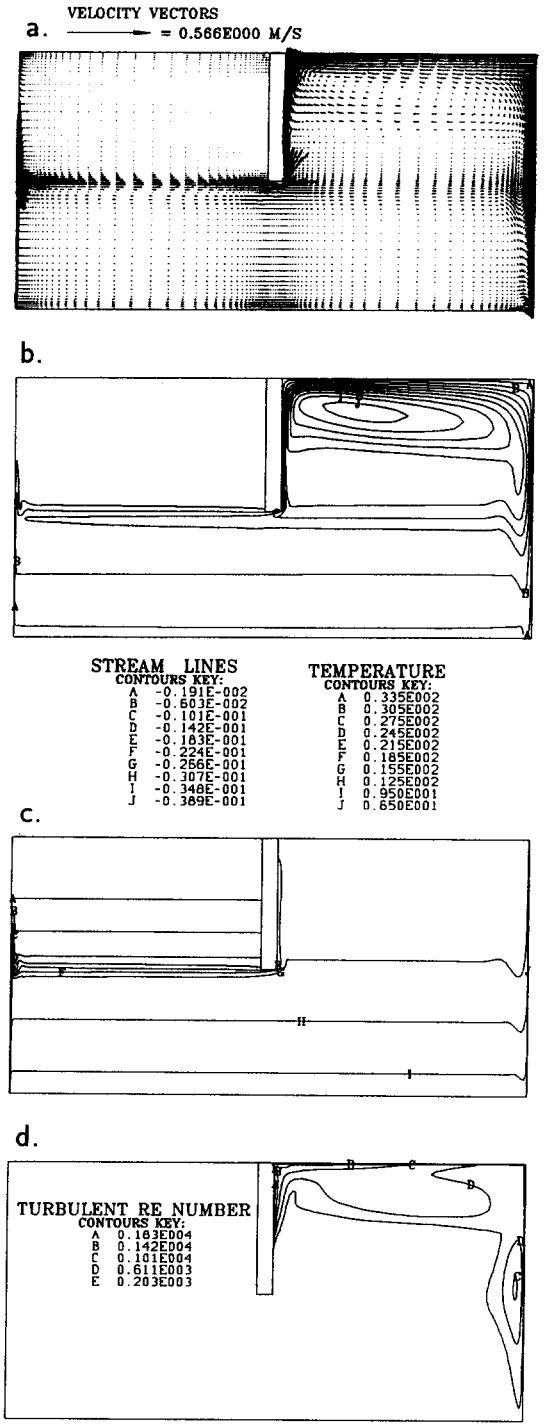

Fig. 8. Computed mean and turbulence properties in a partially divided side heated rectangular enclosure, $H:L = 1:2$, $H_{ob}/H = 0.5$, $Ra_L = 1.2 \times 10^{12}$; (a) velocity vectors; (b) streamlines; (c) isotherms and (d) turbulence Reynolds number, Re_t.

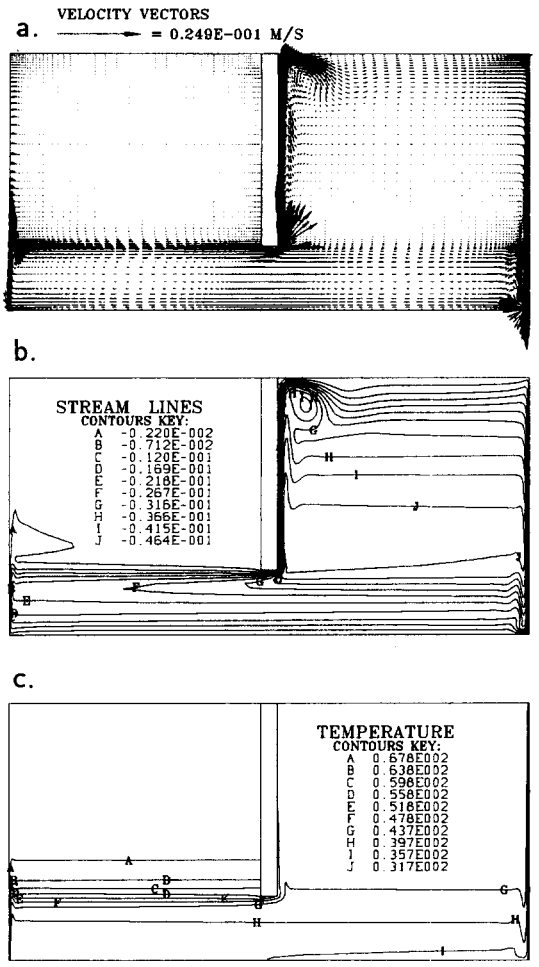

Fig. 9. Computed mean flow properties in a partially divided side heated rectangular enclosure, $H:L = 1:2$, $H_{ob}/H = 0.75$, $Ra_L = 1.2 \times 10^{12}$.

lent, in spite of a relatively high Ra number. However, a strong recirculation is generated in the upper right zone between the partition, ceiling and the cold wall. Although there is no visible separation in this region, an intensive turbulence is generated with turbulence Reynolds number $Re_t = k^2/v\varepsilon$ reaching almost 2000. The turbulence is partly convected down the cold wall where additional production occurs, creating another high Re_t zone at the midheight of the cold wall, with significant temperature fluctuations and a consequent turbulent heat flux, although the kinetic energy is relatively low as compared with that in the corner behind the partition. It should be noted that this pattern very much resembles that observed by Nansteel and Greif [2] in their 3D enclosures with the small breadth opening in the partition.

In the absence of other data for verification of the obtained results we compared the mean temperature and velocity profiles in the two cases with partitions with the measurements of Nansteel and Greif [1] and of Lin and Bejan [4]. Figure 10 shows the comparison of the vertical mean temperature profiles at three stations: below the partition and in the middle of both zones for $H_{ob}/H = 0.5$ and 0.75. In both experiments the flow was laminar. In spite of the fact that our computations yielded turbulence in some parts of the enclosure for $H_{ob}/H = 0.5$ the compared temperature

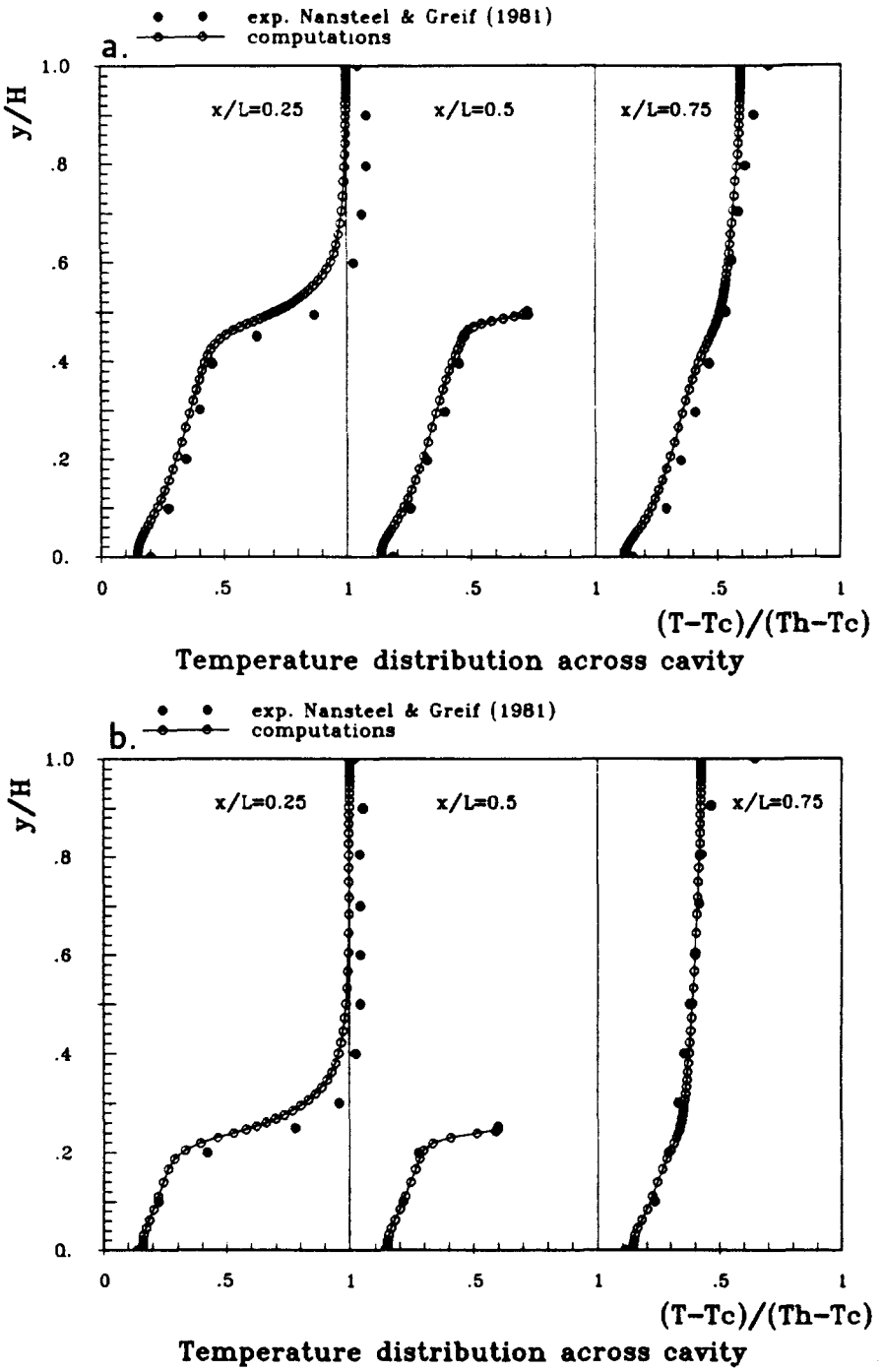

Fig. 10. Comparison of mean temperature profiles in vertical cross-sections in partitioned enclosures, $H:L = 1:2$, $Ra_L = 1.2 \times 10^{12}$: (a) $H_{ob}/H = 0.5$ and (b) $H_{ob}/H = 0.75$.

profiles in both cases considered showed very good agreement. The experimental data in the upper region indicate some heat losses through the upper wall, causing the wall temperature to drop below the maximum fluid temperature. These losses were not accounted for in the computations, hence a discrepancy between the calculated and measured profiles in the upper zone.

Figure 11 shows the computed velocity profiles at selected vertical cross-sections for two cases with $H_{ob}/H = 0.5$ and 0.75, showing in both cases a conspicuous jet across the enclosure at the height just below the partition tip, reaching the maximum velocity at the partition. A counterflow develops below the jet, exhibiting two velocity maxima. An almost identical flow pattern was detected experimentally by

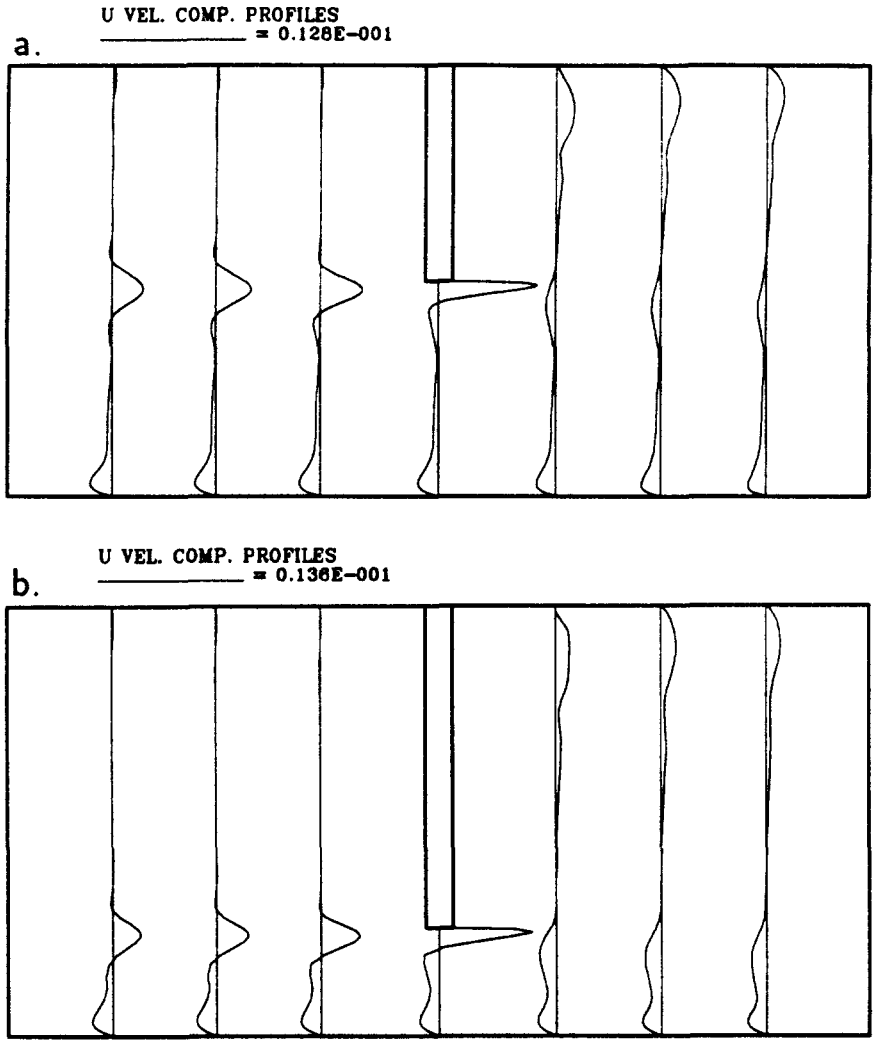

Fig. 11. Computed velocity profiles at selected vertical cross-sections in partitioned enclosures, $H: L = 1:2$, $Ra_L = 1.2 \times 10^{12}$: (a) $H_{ob}/H = 0.5$ and (b) $H_{ob}/H = 0.75$.

Lin and Bejan [4], save for the absolute values, which are different due to the difference in the *Ra* numbers.

The effect of the partition length upon the heat transfer on the non-adiabatic walls is illustrated in Fig. 12 showing the distribution of the Nusselt number along the left and right wall for five different cases of partition height. The laminar-to-turbulent transition, characterized by a sudden increase in the Nusselt number, after a monotonic decrease, is visible for all cases, and corresponds to turbulence iso-contours in the preceding diagrams.

4.4. *Enclosures with a complete conductive partition and mixed boundary conditions*

The last example simulates closely a real situation encountered in space heating: two neighbouring rooms, each 2.6 m high and 3.45 m long, separated by a 0.12 m thick brick wall. The left room is heated from below (floor heating) with constant temperature of 32°C, whereas the right room is cooled through the outer side wall, which is assumed to be at constant temperature of 7.5°C. The reference temperature is 20°C. The resulting Rayleigh number, based on the enclosure height H is $Ra_H = 4.5 \times 10^{10}$. The conductive partition acts as a heat sink for the left room, and as a heat source for the right room, but its temperature is obviously not constant. The resulting flow pattern will depend strongly on the conductivity of the partitioning wall. In order to consider a case with a strong interaction between the two rooms, we have selected a high conductivity wall, with $\lambda = 2.5$ W $m^{-1}K^{-1}$, corresponding to chrome brick or similar material.

Figures 13(a) and (b) show the mean velocity vectors and the mean temperature contours, respectively. Turbulence distribution is illustrated by the contours of the turbulence Reynolds number, turbulent kinetic energy k, temperature variance, $\overline{\theta^2}$, and two components of the turbulent heat flux $\overline{\theta u_1}$ and $\overline{\theta u_2}$, Figs. 13(c) and (e)–(h).

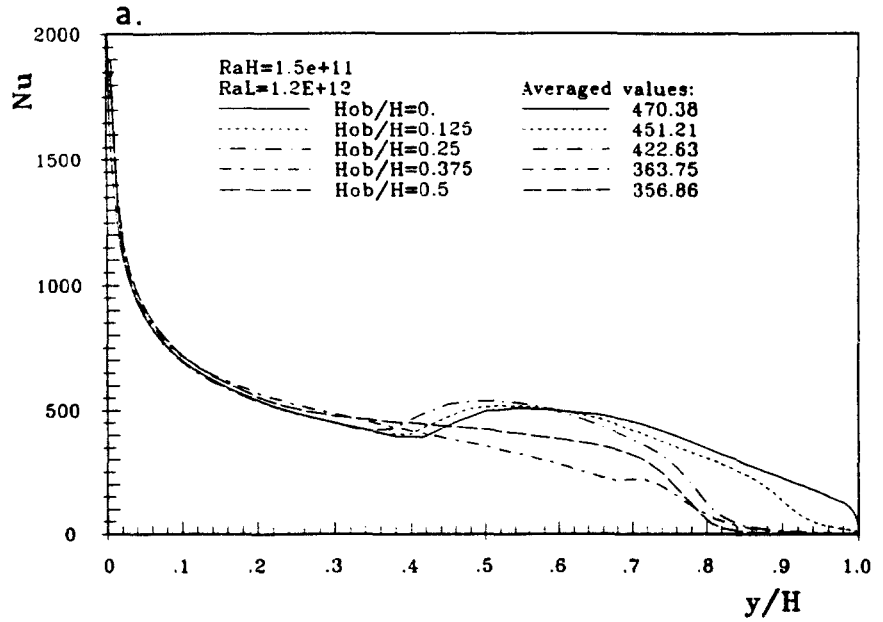

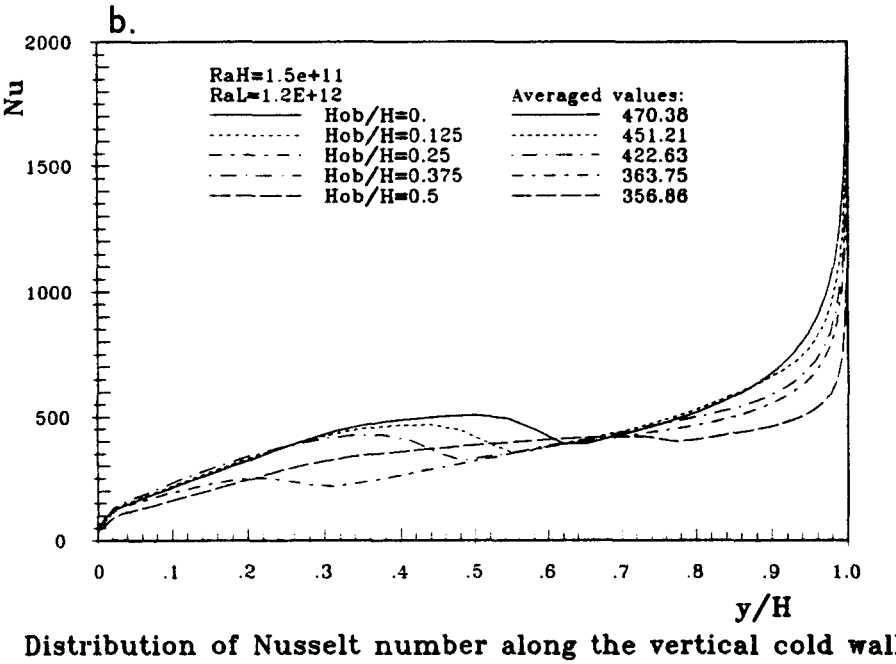

Fig. 12. Nusselt number distribution along non-isothermal walls for enclosures with different partition lengths.

Conductive heat removal along the partition cools the adjacent fluid in the hot room, which accelerates downwards, generating a thin wall-jet type boundary layer and causing a recirculation motion of the fluid along the surrounding walls in the clockwise direction. Heating of the floor enhances this circulation, but the buoyancy in the vertical direction thickens the boundary layer along the horizontal walls, reducing the vertical width of the almost stagnant core. Significant temperature gradients appear in the thin region along the non-adiabatic walls, whereas the rest of the space has an almost constant temperature. Over the larger part of the boundary layer on the floor, excluding the left downstream corner, the temperature profile in the mixed layer above the floor shows an inversion with a steep decrease from the wall temperature $\Theta = (T-T_c)/(T_h-T_c) = 1$ to its minimum $\Theta \approx 0.80$–0.85 in the outer part of the layer, and increases back to the value of about 0.88, which prevails in the rest of the enclosure.

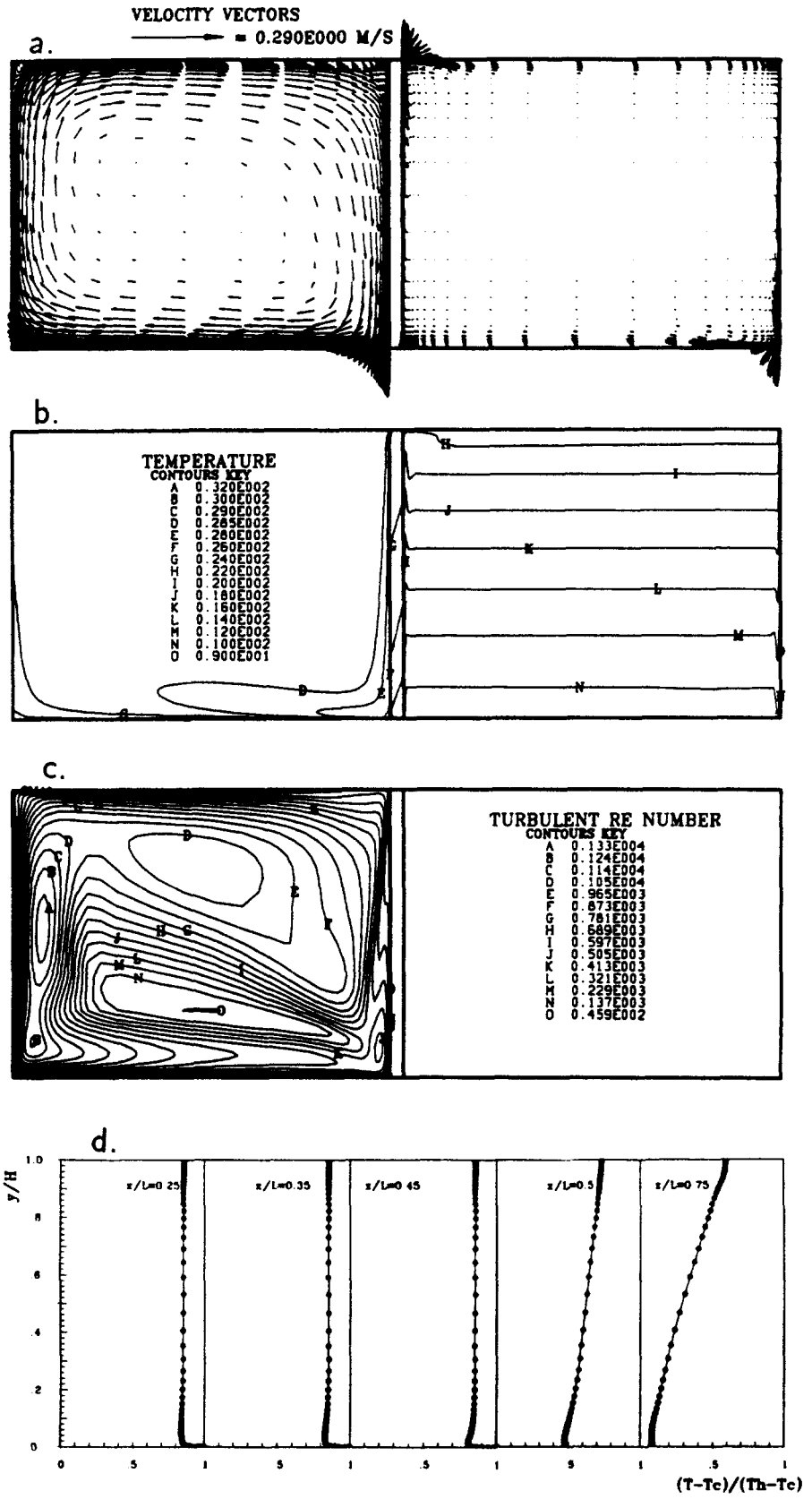

Fig. 13. Mean flow and turbulence properties in a rectangular enclosure with full conductive partition and mixed boundary conditions; $H:L = 1:2.7$, $Ra_H = 4.5 \times 10^{10}$.

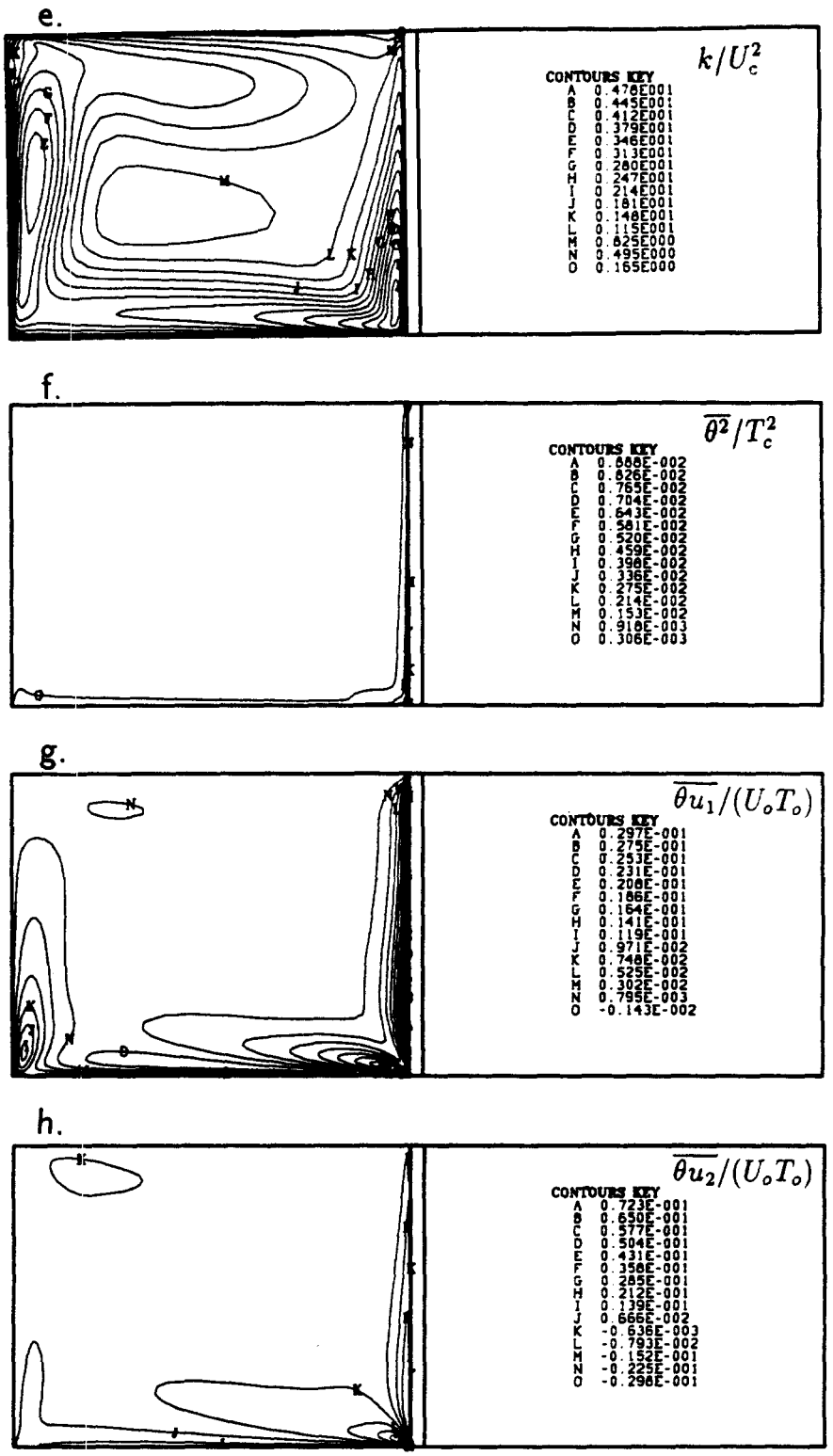

Fig. 13. *Continued.*

The turbulence properties show interesting pattern: the mechanical turbulence of a substantial intensity occupies the whole hot room, whereas the thermal turbulence remains significant only in the vicinity of the non-adiabatic walls. Again, the large length scale in the central portion of the room gives rise to the turbulence Re_t number which is directly proportional to the ratio of the turbulent to molecular viscosity and

therefore is a good indication of the turbulent mixing. However, the velocity fluctuations, which influence the human comfort, take significant values mainly in the wall regions. The temperature variance is confined to even narrower regions adjacent to the non-adiabatic walls.

The flow pattern in the neighbouring room has the characteristics typical for a side heated cavity at low *Ra* numbers, exhibiting a strong temperature stratification with laminar circulation of the fluid in thin boundary layers along the surrounding walls.

4. CONCLUSIONS

The paper presented some results of a computational study of natural convection in undivided and partitioned 2D rectangular cavities with different boundary conditions, simulating real building enclosures. The solutions were obtained by means of an algebraic turbulent flux model, in conjunction with differential transport equations for turbulence energy k, temperature variance $\overline{\theta^2}$ and their dissipation rates ε and ε_θ, as well as with a simpler version of the model in which ε_θ was evaluated on the basis of the assumed constant time scale ratio. The model incorporates the low-*Re*-number modifications and involves the integration up to the wall. The same model was tested earlier in the computation of several simpler test cases with different boundary conditions, yielding satisfactory agreement with available experiments and direct numerical simulation for a range of Rayleigh numbers. The computational results in the present study were also verified by comparison with the available experimental results for the mean temperature and velocity field in some of the considered geometries, with the visual observations of the flow patterns by other researchers, and with the correlations for the Nusselt number. The following major conclusions emerged from the study:

(1) In all cases considered, the applied model gave plausible mean temperature and velocity fields. The computed profiles across the enclosures showed good agreement with the experimental data for all cases for which the data were available in the literature.

(2) The model reproduced the flow patterns and some interesting features in accord with the visual observations reported by several authors for comparable Rayleigh numbers. Of particular relevance to human comfort, fire and smoke spread, or cooling rates in electronic equipment, are the jet like horizontal flow at the partition tip across the partially divided enclosure, and backflow with double velocity maxima below the partition, as well as the counterflow in the outer region of the wall-jet type of the boundary layers along the vertical non-adiabatic walls.

(3) For enclosures filled with air at higher Rayleigh numbers the computations in undivided and partitioned 2D enclosures reproduced a persistent turbulence in some parts of the enclosures in accord with visual detection in experiments. Unlike the conventional eddy diffusivity model, such as low-*Re*-number k–ε model, which reproduced turbulent regime erratically and only at substantially higher *Ra* numbers than observed in experiments, the algebraic flux model proved capable of generating and maintaining the mechanical and thermal turbulence at *Ra* numbers in accord with experimental findings. In cases with side heating and cooling the turbulence was found in regions adjacent to the non-adiabatic walls, influencing substantially the averaged heat transfer across the enclosure.

(4) Comparison with the available data for Nusselt numbers, as well as with the heat transfer correlations for specific cases, showed generally good agreement, which was always within 15%. It is interesting to note that the computed results do not follow a unique relationship $Nu = CRa^n$ over the considered range of *Ra* numbers, as also found by experiments. The agreement with the existing correlations is better at lower *Ra* numbers. In view of the fact that most available correlations were derived by curve fitting through the data obtained at lower *Ra* numbers, this result is expected. For higher *Ra* numbers, where the turbulence occupies larger portion of the enclosures, better agreement was obtained with correlations with higher values of the exponent n (close to 1/3).

(5) In all cases considered, the computations yielded strong variations of the Nusselt number along the non-adiabatic walls, with sudden increase at the onset of turbulence transition, the location of which depends on the *Ra* number. This finding illustrates best the importance of reliable field modelling and computations, which can predict the detailed distribution of the heat transfer coefficient along the walls and detect critical zones with extreme (high or low) heat transfer rates, as well as enable the optimum design of the geometry and heat load for each particular application.

Acknowledgements—Most computations reported in the paper have been performed during the stay of both first-listed authors at the Lehrstuhl für Strömungsmechanik of the Fiedrich-Alexander University, Erlangen-Nuremberg. The authors acknowledge the valuable support of the Deutsche Forschungsgemeinschaft (to K.H.) and of the International Bureau of the Forschungszentrum Jülich (to S.K.).

REFERENCES

1. M. W. Nansteel and R. Greif, Natural convection in undivided and partially divided rectangular enclosures, *J. Heat Transfer* **103,** 623–629 (1981).
2. M. W. Nansteel and R. Greif, An investigation of natural convection in enclosures with two- and three-dimensional partitions, *Int. J. Heat Mass Transfer* **27**(4), 561–571 (1984).
3. S. M. Bajorek and J. R. Lloyd, Experimental investigation of natural convection in partitioned enclosures, *J. Heat Transfer* **104,** 527–531 (1982).
4. N. N. Lin and A. Bejan, Natural convection in a partially divided enclosure, *Int. J. Heat Mass Transfer* **26**(12), 1867–1878 (1983).
5. D. A. Olson, L. R. Glicksman and H. M. Ferm, Steady-

state natural convection in empty and partitioned enclosures at high Rayleigh numbers, *J. Heat Transfer* **112,** 640–647 (1990).
6. K. S. Chen, A. C. Ku and C. H. Chou, Investigation of natural convection in partially divided rectangular enclosures both with and without an opening in the partition plate: measurement results, *J. Heat Transfer* **112,** 648–652 (1990).
7. K. C. Karki, P. S. Sathyamurthy and S. V. Patankar, Natural convection in a partitioned cubic enclosure, *J. Heat Transfer* **114,** 410–417 (1992).
8. J. Neymark, C. R. Boardman and A. Kirkpatrick, High Rayleigh number natural convection in partially divided air and water filled enclosures, *Int. J. Heat Mass Transfer* **32**(9), 1671–1679 (1989).
9. T. Fusegi, J. M. Hyun and K. Kawahara, Numerical simulation of natural convection in a differentially heated cubical enclosure with a partition, *Int. J. Heat Fluid Flow* **13**(2), 176–183 (1992).
10. K. Hanjalić and S. Vasić, Numerical simulation of free convection in single- and multiple-zone rectangular cavities, *Proceedings of the 9th International Heat Transfer Conference*, Vol. 2, pp. 579–584 (1990).
11. K. Hanjalić, S. Kenjereš and F. Durst, Numerical study of natural convection in partitioned two-dimensional enclosures at transitional Rayleigh numbers, *Proceedings of the 10th International Heat Transfer Conference*, Vol. 5, pp. 477–482 (1994).
12. W. P. Jones and B. E. Launder, Prediction of laminarization with a two-equation model of turbulence, *Int. J. Heat Mass Transfer* **15,** 301 (1972).
13. K. Hanjalić and S. Vasić, Some further exploration of turbulence models for buoyancy driven flows, *Turbulent Shear Flows* (Edited by Durst *et al.*), Volume 8, pp. 319–341. Springer, Berlin (1993).
14. N. Z. Ince and B. E. Launder, On the computation of buoyancy driven turbulent flows in rectangular enclosures, *Int. J. Heat Fluid Flow* **10,** 110–117 (1989).
15. I. Demirdžić and M. Perić, Finite volume method for prediction of fluid flow in arbitrary shaped domains with moving boundaries, *Int. J. Numer. Meth. Fluids* **10,** 771–790 (1990).
16. K. Hanjalić and S. Vasić, Computation of turbulent natural convection in rectangular enclosures with an algebraic flux model, *Int. J. Heat Mass Transfer* **36**(14), 306–3624 (1993).
17. T. Y. Chu and R. J. Goldstein, Turbulent convection in a horizontal layer of water, *J. Fluid Mech.* **60,** 141–159 (1973).
18. K. Hanjalić, Achievements and limitations in modelling and computation of buoyant turbulent flows and heat transfer, special keynote paper, *Proceedings of the 10th International Heat Transfer Conference* Brighton, U.K., Vol. 1, pp. 1–18. Institution of Chemical Engineering, London (1994).
19. R. J. Goldstein and T. Y. Chu, Thermal convection in a horizontal layer of air, *Prog. Heat Mass Transfer* **2,** 55–75 (1969).
20. B. Gebhardt, Y. Jaluria, R. L. Mahajan and B. Sammakia, *Buoyancy-induced Flows and Transport*. Hemisphere, New York (1988).
21. M. S. Bohn, A. T. Kirkpatrick and A. D. Olson, Experimental study of three-dimensional laminar convection at high Rayleigh number, *J. Heat Transfer* **106,** 339–345 (1984).